

Predicting bioaccumulation using molecular theory: A machine learning approach

Sergey Sosnin¹, Maksim Misin², Maxim V. Fedorov¹

¹Skolkovo Institute of Science and Technology, Skolkovo Innovation Center, Moscow 143026, Russia

²Institute of Chemistry, University of Tartu, Ravila 14a, Tartu 50411, Estonia

E-mail: m.fedorov@skoltech.ru

Abstract. In this work, we present a new method for predicting bioaccumulation factor of organic molecules. The approach utilizes 3D convolutional neural network (ActivNet4) that uses solvent spatial distributions around solutes as input. These spatial distributions are obtained by a molecular theory called three-dimensional reference interaction site model (3D-RISM). We have shown that the method allows one to achieve a good accuracy of prediction. Our research demonstrates that combination of molecular theories with modern machine learning approaches can be effectively used for predicting properties that are otherwise inaccessible to purely physics-based models.

1. Introduction

Molecular theories such as three-dimensional reference interaction site model (3D-RISM) [1, 2, 3] or molecular density functional theory (MDFT) [4, 5, 6] rely on statistical mechanics derived approximations to estimate the equilibrium distribution of solvent around solvated molecules. In turn, these distributions can be related to the solution properties of solvated molecules [7, 8]. Examples include solvation free energy [9, 10, 11], partial molar volume [3, 12], salting out constants [13], binding free energies [14, 15, 16] and others. However, using purely theoretical approach, it is practically impossible to relate these distributions to the substance’s biological effects, such as toxicity or bioaccumulation.

The above does not mean that solvation structure is not useful for the understanding influence of chemical compounds on the living organisms. On the contrary, the rich information encoded in the solvation shell can be used to understand whether a given compound is hydrophobic or hydrophilic [17], guess if it will be able to pass certain membrane channels [18] or in case solvent contains ions, estimate its affinity towards them [13]. All this information is directly related to compound biological effects but can not be expressed rigorously using equations. On the other hand, the machine learning methods are usually quite good at finding and quantifying these relations.

In this article, we utilize a 3D convolutional neural network (CNN) to estimate bioaccumulation factor in a number of organic molecules. As an input, we use three-dimensional distributions of water around these molecules, obtained using 3D-RISM with Kovalenko-Hirata closure (KH) [19]. Artificial neural networks (ANNs) have been previously used for predicting biological effects of organic molecules [20, 21, 22]. However, they were combined with a very broad set of descriptors that have diverse physical meanings. Here we focus on a single property, solvation shell structure, and attempt to establish its utility. To determine whether a 3D-RISM procedure is necessary we also train electrostatic potential based model and compare the results.

2. Theoretical Background

2.1. Representation of Molecules

In chemical informatics molecules are typically represented using a variety of descriptors. The simplest descriptors are derived from a graph representation of a molecule. Although this is a very compact representation which requires little storage, it ignores a lot of spatial details and can not be used as an input for the majority of neural networks.

The numerical descriptors based on: fragmental [23], topological [24], quantum [25], physicochemical [26] and other properties are more suitable for machine learning approaches and have been used extensively in traditional QSAR/QSPR models. However, typically, accurate models require combining of descriptions of different nature, that makes the interpretation of such models difficult.

An interesting approach to these limitations is offered by 3D QSAR approaches that

can combine a rich numerical description of a molecule with relatively easily interpretable models. One of the most widely used 3D QSAR method is *Comparative Molecular Field Analysis (CoMFA)*[27]. In this method an interaction energy between the molecule and a probe atom [28] is measured for each 3D grid point forming 3D molecular fields. These 3D fields are analysed by a partial least-squares (PLS)[29] regression to build a predictive model. This method is implemented in the popular commercial software *Sybyl-X*[30] and has been widely used in science and pharmaceutical companies in the last 25 years.

The majority of molecules have a number of conformers with different 3D representations. There is no guarantee that low energy conformers obtained from *in-silico* experiments would correspond to the active conformation of a ligand [31]. To overcome this limitation a number of alignment-free methods have been proposed[32], and a batch of multi-dimensional QSAR methodologies have been developed[33], but there is no universal approach. This problem has inspired us to search for a method that can handle multiple conformations of a molecule.

2.2. 3D Reference Interaction Site Model (3D-RISM)

Calculation of an equilibrium distribution of solvent around an arbitrary molecule is a challenging problem in molecular modeling [3]. It can be done using molecular dynamics simulation, but extremely long simulation times are needed to obtain smooth solvent distributions [34]. MDFT method[6], proposed by Borgis and ER-Theory [35] developed by Matubayasi and Nakahara can be applied to this problem. As an alternative to the molecular simulations, molecular solvation theories (that are also referred to as integral equation theories) offer a less computationally expensive way of calculating the 3D solvation structure around a molecule [3, 36]. One of these methods, a three-dimensional reference interaction site model (3D-RISM) became very popular for calculations of the distribution of solvent sites (atoms) around the molecular solute[3, 19, 37].

As a result of 3D-RISM calculations, one obtains a single-site *density distribution function* (local density) $\rho_\gamma(\mathbf{r})$ of the solvent site γ around the solute molecule. We used a 3-point model of water (SPC/E) meaning that the calculation produces density distributions for both oxygen and hydrogen atoms. These density distributions can be regarded as a variant of molecular fields that we discussed in the previous section. Notice that the densities obtained from RISM calculations are not exact [2, 12], but can be successfully used to predict variety of both chemical and biological properties using either semi-empirical corrections [11, 13, 38, 39, 39] or QSPR approaches [40].

The 3D-RISM main equation can be written as [2, 12]:

$$h_\gamma(\mathbf{r}) = \sum_{\alpha=1}^{n_s} (\chi_{\alpha\gamma} * c_\alpha)(\mathbf{r}),$$

where $*$ denotes convolution, n_s stands for the number of solvent sites, and $h_\gamma(\mathbf{r}) = \rho_\gamma(\mathbf{r})/\rho_\gamma - 1$, usually referred to as the total correlation function, is a function introduced

for convenience. $c(\mathbf{r})$ is a direct correlation function that can be defined via $c_\gamma(\mathbf{r}) = -\mu_\gamma^*(\mathbf{r})/(kT)$. Here k is the Boltzmann constant, T is temperature, and $\mu_\gamma^*(\mathbf{r})$ is an excess chemical potential (relative to ideal gas) of the solvent site γ . Finally, $\chi_{\alpha\gamma}(r)$ is a site-site susceptibility function that can be obtained from a bulk solvent radial distribution functions. More conveniently, $\chi_{\alpha\gamma}$ can be calculated from a separate 1D-RISM calculation[3, 41].

The above equation is usually coupled with a separate closure relation that provides another connection between $h_\gamma(\mathbf{r})$ and $c_\alpha(\mathbf{r})$. In this work we used a simple, but robust *Kovalenko-Hirata (KH)*[42] closure:

$$h_\gamma(\mathbf{r}) + 1 = \begin{cases} \exp[-\beta u_\gamma(\mathbf{r}) + h_\gamma(\mathbf{r}) - c_\gamma(\mathbf{r})], & \text{if } h(\mathbf{r}) \leq 0; \\ 1 - \beta u_\gamma(\mathbf{r}) + h_\gamma(\mathbf{r}) - c_\gamma(\mathbf{r}), & \text{if } h(\mathbf{r}) > 0; \end{cases}$$

where $\beta = 1/(kT)$ and $u_\gamma(\mathbf{r})$ is a potential energy between the solvent site γ and the solute molecule. Together the above systems of equations are usually iteratively solved until both $h_\gamma(\mathbf{r})$ and $c_\alpha(\mathbf{r})$ achieve the predefined convergence criteria.

2.3. Bioconcentration factor (BCF)

In this work, we built a model for predicting the bioconcentration factor, BCF (more specifically, we predicted its decimal logarithm $\log_{10}\text{BCF}$). This factor is the ratio between the concentration of an organic compound in biota and in water:[43]

$$\text{BCF} = \frac{\text{Concentration}_{\text{biota}}}{\text{Concentration}_{\text{water}}} \quad (1)$$

This factor is an important parameter for estimating the potential danger of an organic compound. It is one of the parameters that determine the labeling of the compound under *Registration, Evaluation, Authorisation and Restriction of Chemicals (REACH)* program in European Union. The ability of a compound to penetrate and conserve in an organism may influence the toxicity and mutagenicity of the compound, and so may reveal potential environmental risks. Generally, if a compound has BCF value of more than 5000 (or $\log_{10}\text{BCF} > 3.67$), it is regarded as potentially dangerous. There are several methods to measure and estimate the confidence of the BCF data, described in details in ref. 44. The detailed description of BCF estimation is published in Organisation for Economic Cooperation and Development (OECD) guideline No 305[45]. It should be textitized that determining of BCF in in-vivo experiments is a very expensive procedure.

Over the years, several models for BCF prediction have been published. Arnot and Gobas have proposed a linear model that predicted BCF as a function of the uptake and elimination of an organic compound by an aquatic organism. Since BCF is related to $\log P$ and water solubility[44], some authors proposed models that utilise these descriptors [46]. These linear models work satisfactory only for moderately hydrophobic compounds, but fail to address strongly hydrophobic chemicals[47]. Additionally, $\log P$ is a parameter that must be measured separately and this may be problematic. Another

notable model has been produced by Zhao et al.[48] using a hybrid of a number of machine learning methods. Their model managed to produce an impressive accuracy ($R^2 = 0.8$, RMSE = 0.59), albeit on a somewhat curated dataset.

To conclude the above, modeling of the bioconcentration factor is an important research area due to the difficulties associated with its experimental evaluation and importance of such models for regulatory purposes.

3. Methods and Materials

Databases We used the dataset collected by USA Environmental Protection Agency for their T.E.S.T. QSAR platform for risk estimation[49]. This dataset has been split into training and test subsets in the same manner as it was done by US EPA, and statistical values on the test set are published. We used them as a baseline for our model. There are 541 molecules in the training set and 135 molecules in the test set.

We used rdkit[50], an open-source cheminformatic toolkit, to perform basic molecular routines and to calculate the geometries of molecules.

Conformers Generations For deep neural networks, high amount of diverse data is a key factor to success. Our approach to conformer generation and selection is similar to the method from the article[51] and is briefly described below.

At the first stage of the algorithm, we generate a number of conformers by rotating the bonds of a molecule. This is followed by an energy minimization step, consisting of 5000 iterations and performed using the universal force field (UFF) [52]. Subsequently, all conformers with RMSD (computed on the heavy atoms) of less than 0.5 Å are discarded. If the number of conformers exceeds the pre-defined limit, then the post-processing procedure from paper[51] is performed (we discuss this procedure in more details in the Supporting Information).

Force field assignment We used AmberTools16[53] package to calculate the partial charges of each molecule using AM1-BCC[54] semi-empirical model. At this stage, for some molecules from the training set the calculations have not converged, and these molecules were eliminated. These partial charges were used for further 3D-RISM calculations and for the evaluation of electric potential fields.

Electric potential field We calculated the electrostatic potential around every molecule by placing it into a cube box (voxel grid) with the dimensions of 35 Å × 35 Å × 35 Å using a grid with the step size of 0.5 Å for all dimensions. For each grid point j in the 70 × 70 × 70 box we calculated

$$U_j = \frac{1}{4\pi\epsilon_0} \sum_i^{atoms} \frac{q_i}{|\mathbf{r}_{ij}|}$$

Where ϵ_0 stands for the vacuum permittivity, q_i is a partial charge of the i -th solute atom and $|\mathbf{r}_{ij}|$ is the distance between the atom i and the grid point j .

We implemented the code for the potential calculation on GPU units using framework *cupy* (a part of *chainer* framework[55]), and used it for “on-the-fly” 3D fields

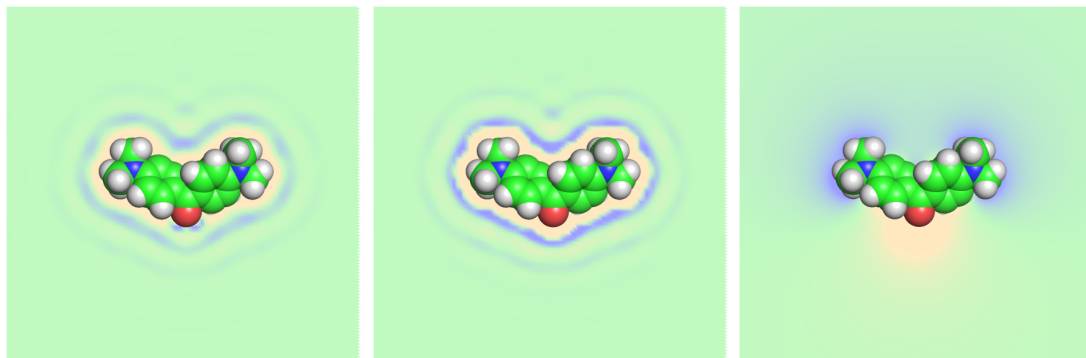


Figure 1: An example of the visualization of the scalar fields for a molecule as 2D slices taken by the principal axis (Left – a visualization of hydrogens density. Center – a visualization of oxygen density. Right – a visualization of electric field. light yellow color – lower values, pale green color – values at the edges of the boxes, blue color – higher values))

calculation. Note that before being fed to the neural network, all values of the potential were scaled by a constant factor to scale it into a reasonable range.

Lennard-Jones potential field We calculated the Lennard-Jones potential field in the similar manner to electric potential described above. For each atom pairs ϵ and σ parameters have been taken and mixed with a probe atom in accordance with *GAFF2* forcefield[53] mixing rules. We used oxygen bonded with hydrogen as probing atom (noted as “oh” in *AmberTools*) to make the modeling routine close to potential estimation with water as a solvent in RISM.

$$U_j = 4\epsilon_{ij} * \sum_i^{atoms} \left(\left(\frac{\sigma_{ij}}{|\mathbf{r}_{ij}|} \right)^{12} - \left(\frac{\sigma_{ij}}{|\mathbf{r}_{ij}|} \right)^6 \right)$$

We clipped values of energies more than 2 *kcal/mol* to precise 2 *kcal/mol*. and less than zero to zero to avoid numerical dispersion. It was established in our research that smoothing Lennard-Jones potentials is a crucial step, and we transformed the values by e^{-U} in every grid point.

3D-RISM Calculations 3D-RISM equation was solved using *rism3d.snglpnt* program from *AmberTools16*[53] package. Water with temperature 298 K was used as a solvent. Site-site susceptibility functions of bulk water ($\chi_{\alpha\gamma}(\mathbf{r})$) were calculated using DRISM method by *drism* program from the same package. For 3D-RISM we used a $35 \text{ \AA} \times 35 \text{ \AA} \times 35 \text{ \AA}$ grid with 0.5 \AA step size. The resulting oxygen and hydrogen density distributions were saved as HDF5[56] binary files. We ran a separate 3D-RISM calculation for each conformer. If more than 50% of 3D-RISM calculations did not converge, the molecule was marked as “failed” and was eliminated from the dataset.

3D Convolutional Neural Networks Modeling Procedure We used framework *chainer*[55] to build networks for processing 3D data. The architecture of the network is schematically presented in figure 2 (a more standard representation is provided in table

S1 in the Supporting Information). This architecture was optimal in terms of speed and the quality of the training models. This model has been called *ActivNet4*, with four indicating the number of convolutional layers used.

We trained this network on 3D fields using electric potentials and 3D-RISM results. Since we used water as a solvent in 3D-RISM calculations, we had two input channels (H and O atoms) in the 3D-RISM data, but only one in case of electric potentials.

We used *Parametric Rectified Linear Units*[58] as activation functions in the model, because they showed small improvement on the quality although it is possible to replace them with the common *relu* activation function without noticeable lack of performance. To train *ActivNet4*, we experimented with several optimizers: Stochastic gradient descent with momentum, *Adam*[59], *RMSprop*[60], and *SMORMS3*[61]. The best and stable convergence has been provided by *SMORMS3* method. *RMSprop* and *Adam* have a good convergence ability, but the training process was less stable. Stochastic gradient descent has converged noticeably more slowly for the network. The parameters of the optimisers can be found in the Supporting Information.

The training and test processes were slightly different. At the training stage, each conformer of the molecule has been regarded independently from the other conformers. At the test stage, the prediction value for each conformer of the molecule has been calculated and the final result was the mean value for all conformers of the molecule. The performance of the model was estimated on the same test set that has been used in the original work to compare our model with the baseline. Further, we used 5-fold cross-validation (CV) technique to account the quality of the model in a more trusted way. The Neural networks have been trained using Nvidia K80 graphics cards and Nvidia GTX 1080 cards.

Extreme Gradient Boosting modeling To compare our 3D convolutional network with other machine learning approaches we built models using Extreme Gradient Boosting (XGBoost implementation[62]) algorithm. This method has been proposed for use in cheminformatics[63] and can process very large datasets rapidly and efficiently. In this experiment, initially, we had to decrease the volume of each 3D cube from $70 \times 70 \times 70$ to $17 \times 17 \times 17$ by performing the average pooling operation with a kernel $(4, 4, 4)$. Then, both oxygen and hydrogen channels have been flattened and stacked forming a vector of 9826 values. These vectors served as the inputs for XGBoost algorithm. The application of the method to the test set has been performed in the same manner as in the neural network experiment. We used the maximal number of trees = 100 and maximal depth of each tree = 6 to train the models, the other parameters have been set to default.

4. Results and Discussion

Our main goal was to evaluate whether it is possible to predict biological property using a combination of solvation structure and machine learning. For this we took 670 molecules with known bioaccumulation constants and split them into a training (537 molecules) and test (133 molecules) sets. For each molecule we then generated a diverse

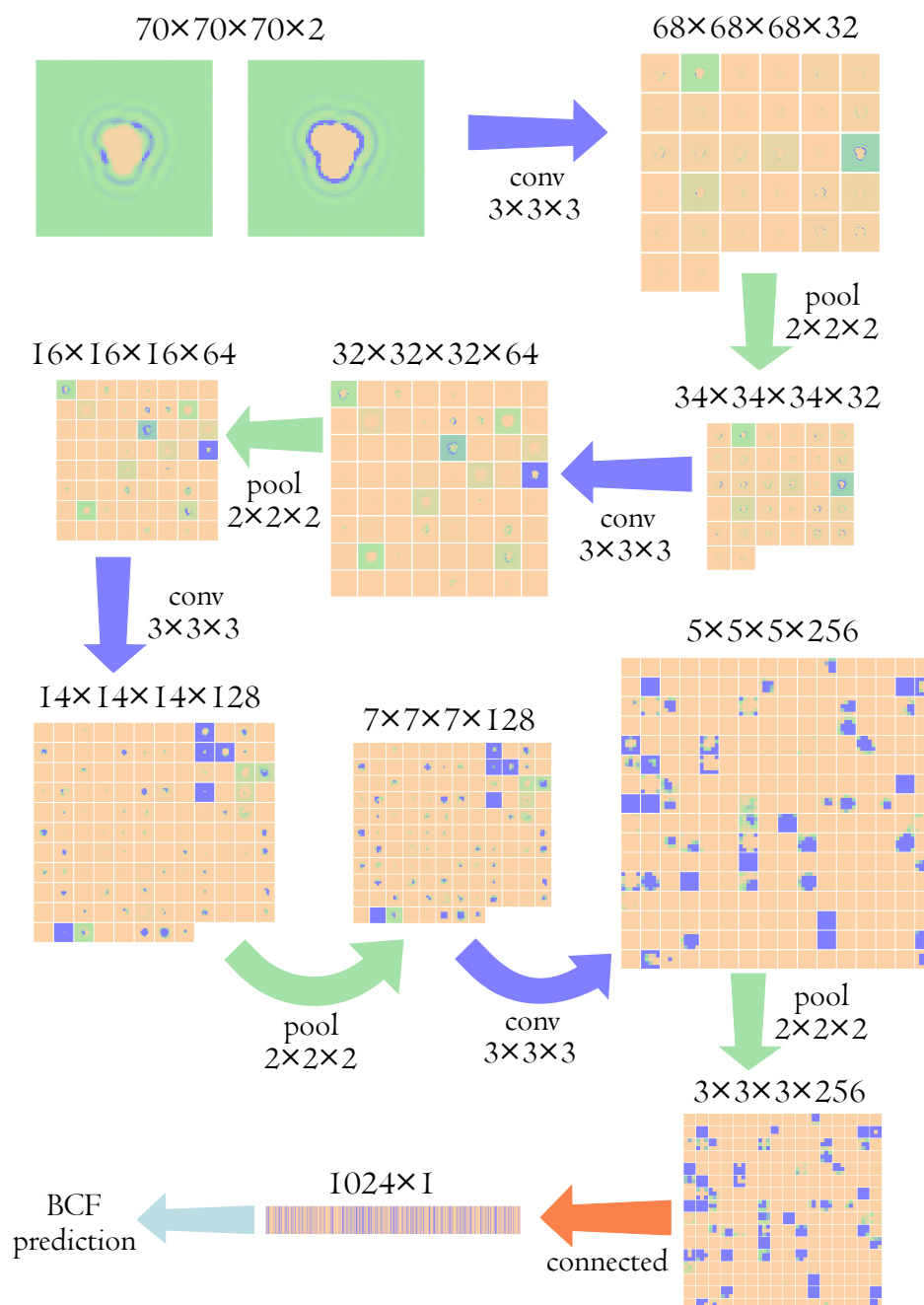


Figure 2: A schematic representation of *ActivNet4* architecture with visualized 2D slices of feature maps on a trained network. Feature maps are colored using the same color scheme as in figure 1. Blue arrows labeled $\text{conv } N \times N \times N$ denote a 3D convolution layer, green arrows labeled $\text{pool } N \times N \times N$ denote 3D max-pulling layer, and red arrow labeled "connected" denotes a fully-connected layer. The figure is based on figure 4 from Ref. 57

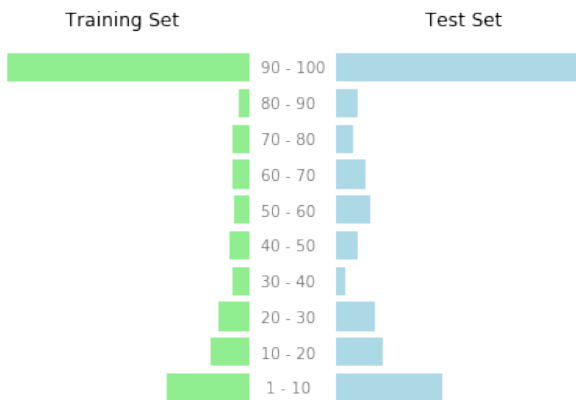


Figure 3: The distributions of the number of conformers for each molecule in the training and test sets

Table 1: Accuracies of \log_{10} BCF predictions by different models. RMSE stands for root mean square error, MAE stands for mean absolute error and R denotes Pearson’s correlation coefficient.

Model		RMSE	MAE	R ²
US EPA (baseline)	consensus model	0.66	0.51	0.76
	single model	0.68	0.64	0.74
ActivNet4 (3D-RISM)	training/test	0.66	0.48	0.77
	5-fold CV	0.65	0.48	0.77
ActivNet4 (electric potential)	training/test	0.72	0.53	0.72
	5-fold CV	0.72	0.54	0.72
ActivNet4 (Lennard-Jones potential)	training/test	1.03	0.81	0.42
	5-fold CV	1.07	0.86	0.38
ActivNet4 (Lennard-Jones and electric potentials)	training/test	0.70	0.51	0.73
	5-fold CV	0.66	0.49	0.76
XGBoost (3D-RISM)	training/test	0.85	0.70	0.61
	5-fold CV	0.91	0.72	0.54

set of conformers, using an earlier described procedure. The distribution of a number of conformers for both training and test set is shown in figure 3.

Figure 3 shows that about a quarter of the molecules in the training and test sets have less than 10 conformers (quite inflexible), while the rest consists of highly flexible molecules with 90-100 conformers. The distribution of the conformers is similar for the train and test sets.

The main result of the paper is presented in Table 1. As one can see, the ActivNet4 model has been capable of achieving a quality comparable to the “consensus” model provided by US EPA[49]. This result is noteworthy due to the fact that our model was based only on the 3D distribution of water molecules while the EPA’s models used a

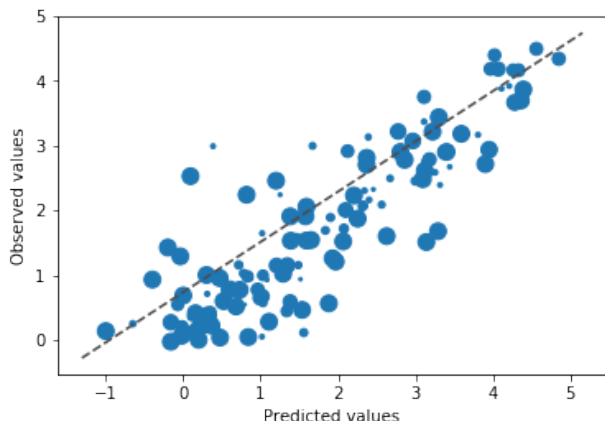


Figure 4: Correlation between observed and predicted values of \log_{10} BCF. The size of the marker depends on the number of conformers of the molecule.

large set of descriptors of varying nature. The comparison of the two models reveals that the analysis of solvent density distributions using 3D Convolutional neural networks may be useful for predicting biological properties. In addition, we demonstrate that the distribution can be correlated with the bioconcentration factor.

We compared the results obtained by RISM, electric and Lennard-Jones potentials fields. The quality of models on the base of RISM is slightly higher than ones built on electric field and notably higher than ones, based on Lennard-Jones potential. It can be interpreted, that taking into account solvation effects have an important role in bioconcentration processes. The question of why the qualities of models on the base of Lennard-Jones potentials fields has less quality than the models based on electric potentials should be explained in the future researches.

One of the problems in our approach is related to the complexity of its set up. Indeed, both 3D-RISM calculations as well as 3D convolutional neural networks require some expertise to utilize. To check whether either of these procedures is necessary we also trained our network on electric potentials of molecules (third row in table 1) as well as used 3D-RISM obtained fields in combination with Extreme Gradient Boosting (XGBoost, fourth row of the table) algorithm. Both alternatives demonstrated worse results compared to the original, indicating that both 3D-RISM as well as CNN-s are necessary to achieve accurate results. Additionally, to address the difficulty of the codes we created a convenient script to simplify whole procedure, located on github [64].

Another bottleneck of the proposed techniques is the size of the 3D fields. For a $70 \times 70 \times 70$ point 3D grid one has to spend a minimum of $4 \text{ B} \cdot 70^3 = 1\,372\,000 \text{ B}$ (1.31 MB) to store it. In the case of an n -site model of the solvent coupled with an m conformer representation of the solute we arrive to $4 \text{ B} \cdot 70^3 \cdot m \cdot n$ bytes necessary for each molecule.

To reduce the space requirements one can turn towards lossy compression methods for 3D fields. 3D autoencoders seem to be a good choice for this purpose. Another

way is to develop of a method for generating 3D fields “on-the-fly” just before the training iteration. For instance, electric potentials used in this study were generated using quick GPU procedure that was essentially instantaneous (further details available in the supporting information).

5. Conclusions

The aim of the paper was to demonstrate that average solvent distribution in the neighbourhood of solutes can be used in combination with machine learning algorithms to predict properties that do not necessarily follow from the solvation structure alone. In order to achieve it we decided to focus on predicting the bioaccumulation factor using an approximate solvent density obtained using 3D-RISM method of integral equation theories. After training, the *ActivNet4* (4-layer convolutional neural network) managed to predict $\log_{10}\text{BCF}$ from water density distribution with RMSE=0.66. Although the model used relatively simple 3D descriptors, it managed to achieve prediction accuracies that are comparable to the state of the art models.

Despite successful first results, the presented method requires further development. The first task that authors are working on right now is the application of the method to other molecular properties that are difficult to measure. Additionally, it is useful to explore possibilities of integrating solvation shell calculations and training steps to avoid storage limitations. Finally, given a clear physical meaning of the descriptors used in this study, it would be useful to explore precisely which molecular features significantly affect BCF. We hope to answer these and other questions in a follow-up article.

The source code for the 3D fields generation is located on Zenodo doi: 10.5281/zenodo.835526 and GitHub <https://github.com/sergsb/clever>. It is distributed under Apache License 2.0.

6. Acknowledgements

HPC calculations have been performed on Skoltech Pardus cluster. *Instant JChem* was used for structure database management[65]. Computations on GPU was carried out using computing resources of the federal collective usage center “Complex for simulation and data processing for mega-science facilities” at NRC “Kurchatov Institute”. Authors acknowledgment Yermek Karpushev, Evgeny Burnaev, Alexey Zaytsev and David Palmer for fruitful discussions.

References

- [1] Beglov D and Roux B 1997 *J. Phys. Chem.* **101** 7821–7826
- [2] Hirata F 2003 *Molecular Theory of Solvation* (New York: Kluwer Academic Publishers) URL <http://www.springer.com/chemistry/electrochemistry/book/978-1-4020-1562-5>

- [3] Ratkova E L, Palmer D S and Fedorov M V 2015 *Chem. Rev.* **115** 6312–6356 ISSN 0009-2665 URL <http://dx.doi.org/10.1021/cr5000283>
- [4] Jeanmairet G, Levesque M, Vuilleumier R and Borgis D 2013 *J. Phys. Chem. Lett.* **4** 619–624 ISSN 1948-7185 URL <http://dx.doi.org/10.1021/jz301956b>
- [5] Ramirez R and Borgis D 2005 *J. Phys. Chem. B* **109** 6754–6763 ISSN 1520-6106 URL <http://dx.doi.org/10.1021/jp045453v>
- [6] Gendre L, Ramirez R and Borgis D 2009 *Chemical Physics Letters* **474** 366–370 ISSN 0009-2614 URL <http://www.sciencedirect.com/science/article/pii/S0009261409004175>
- [7] Hansen J P and McDonald I R 2013 *Theory of Simple Liquids, Fourth Edition: with Applications to Soft Matter* 4th ed (Amstersdam: Academic Press) ISBN 978-0-12-387032-2
- [8] Ben-Naim A 2006 *Molecular Theory of Solutions* (Oxford: OUP) ISBN 978-0-19-929969-0
- [9] Du Q H, Beglov D and Roux B 2000 *J. Phys. Chem. B* **104** 796–805
- [10] Palmer D S, Frolov A I, Ratkova E L and Fedorov M V 2010 *J. Phys.: Condens. Matter* **22** 492101 ISSN 0953-8984 URL <http://iopscience.iop.org/0953-8984/22/49/492101>
- [11] Misin M, Fedorov M V and Palmer D S 2015 *J. Chem. Phys.* **142** 091105 ISSN 0021-9606, 1089-7690 URL <http://scitation.aip.org/content/aip/journal/jcp/142/9/10.1063/1.4914315>
- [12] Misin M 2017 arXiv: 1704.05246 URL <http://arxiv.org/abs/1704.05246>
- [13] Misin M, Vainikka P, Fedorov M V and Palmer D S 2016 *J. Chem. Phys.* **145** Manuscript Accepted
- [14] Genheden S, Luchko T, Gusarov S, Kovalenko A and Ryde U 2010 *J. Phys. Chem. B* **114** 8505–8516 ISSN 1520-6106 URL <http://dx.doi.org/10.1021/jp101461s>
- [15] Gussregen S, Matter H, Hessler G, Lionta E, Heil J and Kast S M 2017 *J. Chem. Inf. Model.* **57** 1652–1666 ISSN 1549-9596 URL <http://dx.doi.org/10.1021/acs.jcim.6b00765>
- [16] Sugita M and Hirata F 2016 *J. Phys.: Condens. Matter* **28** 384002 ISSN 0953-8984 URL <http://stacks.iop.org/0953-8984/28/i=38/a=384002>
- [17] Lum K, Chandler D and Weeks J D 1999 *J. Phys. Chem. B* **103** 4570–4577 ISSN 1520-6106 URL <http://dx.doi.org/10.1021/jp984327m>
- [18] Roux B and Karplus M 1991 *Biophysical Journal* **59** 961–981 ISSN 0006-3495 URL <http://www.sciencedirect.com/science/article/pii/S0006349591823116>
- [19] Kovalenko A and Hirata F 1999 *J. Chem. Phys.* **110** 10095–10112
- [20] Myint K Z, Wang L, Tong Q and Xie X Q 2012 *Molecular Pharmaceutics* **9** 2912–2923 pMID: 22937990 (*Preprint* <http://dx.doi.org/10.1021/mp300237z>) URL <http://dx.doi.org/10.1021/mp300237z>

- [21] Ajmani S and Viswanadhan V N 2013 *Current Computer-Aided Drug Design* **9** 482–490 ISSN 1573-4099/1875-6697 URL <http://www.eurekaselect.com/node/116577/article>
- [22] Ma J, Sheridan R P, Liaw A, Dahl G E and Svetnik V 2015 *Journal of Chemical Information and Modeling* **55** 263–274 pMID: 25635324 (*Preprint* <http://dx.doi.org/10.1021/ci500747n>) URL <http://dx.doi.org/10.1021/ci500747n>
- [23] Varnek A 2011 *Fragment Descriptors in Structure–Property Modeling and Virtual Screening* (Totowa, NJ: Humana Press) pp 213–243 ISBN 978-1-60761-839-3 URL http://dx.doi.org/10.1007/978-1-60761-839-3_9
- [24] Ivanciuc O 2013 *Current Computer-Aided Drug Design* **9** 153–163 ISSN 1573-4099/1875-6697 URL <http://www.eurekaselect.com/node/111576/article>
- [25] Karelson M, Lobanov V S and Katritzky A R 1996 *Chemical Reviews* **96** 1027–1044 (*Preprint* <http://dx.doi.org/10.1021/cr950202r>) URL <http://dx.doi.org/10.1021/cr950202r>
- [26] Raevsky O A 2004 *Mini-Reviews in Medicinal Chemistry* **4** 1041–1052 ISSN 1389-5575/1875-5607 URL <http://www.eurekaselect.com/node/80232/article>
- [27] Cramer R D, Patterson D E and Bunce J D 1988 *Journal of the American Chemical Society* **110** 5959–5967 pMID: 22148765 (*Preprint* <http://dx.doi.org/10.1021/ja00226a005>) URL <http://dx.doi.org/10.1021/ja00226a005>
- [28] Kubinyi H E (ed) 1993 *3D QSAR in Drug Design* (Springer)
- [29] Wold S, Sjoestrom M and Eriksson L 2001 *Chemometrics and Intelligent Laboratory Systems* **58** 109 – 130 ISSN 0169-7439 pLS Methods URL <http://www.sciencedirect.com/science/article/pii/S0169743901001551>
- [30] Sybyl-x accessed: May 05, 2017 URL <https://support.certara.com/software/molecular-modeling-and-simulation/sybyl-x/>
- [31] Zhang S, Lin Z, Pu Y, Zhang Y, Zhang L and Zuo Z 2017 *Computational Biology and Chemistry* **67** 38–47 ISSN 1476-9271 URL <http://www.sciencedirect.com/science/article/pii/S1476927115301389>
- [32] Myint K Z and Xie X Q 2010 *Int J Mol Sci* **11** 3846–3866 ISSN 1422-0067 URL <http://www.ncbi.nlm.nih.gov/pmc/articles/PMC2996787/>
- [33] Andrade C H, Pasqualoto K F M, Ferreira E I and Hopfinger A J 2010 *Molecules* **15** 3281–3294 ISSN 1420-3049 URL <http://www.mdpi.com/1420-3049/15/5/3281>
- [34] Luchko T, Gusarov S, Roe D R, Simmerling C, Case D A, Tuszynski J and Kovalenko A 2010 *J. Chem. Theory Comput.* **6** 607–624 ISSN 1549-9618 PMID: 20440377 PMCID: PMC2861832 URL <http://www.ncbi.nlm.nih.gov/pmc/articles/PMC2861832/>
- [35] Matubayasi N and Nakahara M 2000 *The Journal of Chemical Physics* **113** 6070–6081 ISSN 0021-9606 URL <http://aip.scitation.org/doi/abs/10.1063/1.1309013>

- [36] Chandler D, McCoy J D and Singer S J 1986 *J. Chem. Phys.* **85** 5971–5976
- [37] Kovalenko A and Hirata F 2000 *J. Chem. Phys.* **112** 10391–10402 ISSN 0021-9606, 1089-7690 URL <http://scitation.aip.org/content/aip/journal/jcp/112/23/10.1063/1.481676>
- [38] Truchon J F, Pettitt B M and Labute P 2014 *J. Chem. Theory Comput.* **10** 934–941 ISSN 1549-9618 URL <http://dx.doi.org/10.1021/ct4009359>
- [39] Misin M, Fedorov M V and Palmer D S 2016 *J. Phys. Chem. B* **120** 975–983 ISSN 1520-6106 URL <http://dx.doi.org/10.1021/acs.jpcb.5b10809>
- [40] Palmer D S, Misin M, Fedorov M V and Llinas A 2015 *Mol. Pharmaceutics* **12** 3420–3432 ISSN 1543-8384 URL <http://dx.doi.org/10.1021/acs.molpharmaceut.5b00441>
- [41] Perkyns J S and Pettitt M B 1992 *Chemical Physics Letters* **190** 626–630 ISSN 0009-2614 URL <http://www.sciencedirect.com/science/article/pii/000926149285201K>
- [42] Kovalenko A and Hirata F 2000 *The Journal of Chemical Physics* **113** 2793–2805
- [43] Arnot J and Gobas F 2003 *QSAR & Combinatorial Science* **22** 337–345 ISSN 1611-0218 URL <http://dx.doi.org/10.1002/qsar.200390023>
- [44] Arnot J A and Gobas F A 2006 *Environmental Reviews* **14** 257–297
- [45] OECD 2012 Paris URL [/content/book/9789264185296-en](http://www.oecd.org/content/book/9789264185296-en)
- [46] Papa E, Dearden J and Gramatica P 2007 *Chemosphere* **67** 351–358 ISSN 0045-6535 URL <http://www.sciencedirect.com/science/article/pii/S0045653506012732>
- [47] Gramatica P and Papa E 2005 *QSAR & Combinatorial Science* **24** 953–960 ISSN 1611-0218 URL <http://dx.doi.org/10.1002/qsar.200530123>
- [48] Zhao C, Boriani E, Chana A, Roncagliani A and Benfenati E 2008 *Chemosphere* **73** 1701–1707 ISSN 0045-6535 URL <http://www.sciencedirect.com/science/article/pii/S0045653508011922>
- [49] 2016 User’s guide for t.e.s.t.(toxicity estimation software tool) accessed: May 05, 2017 URL <https://www.epa.gov/sites/production/files/2016-05/documents/600r16058.pdf>
- [50] Rdkit: Open-source cheminformatics accessed: May 05, 2017 URL <http://www.rdkit.org>
- [51] Jean-Paul E, Garrett M and Charlotte D 2012 *Journal of Chemical Information and Modeling* **52** 1146–1158 pMID: 22482737
- [52] Rappe A K, Casewit C J, Colwell K S, Goddard W A and Skiff W M 1992 *Journal of the American Chemical Society* **114** 10024–10035 (*Preprint* <http://dx.doi.org/10.1021/ja00051a040>) URL <http://dx.doi.org/10.1021/ja00051a040>
- [53] Case D, Betz R, Botello-Smith W, Cerutti D, TE Cheatham I, Darden T, Duke R, Giese T, Gohlke H, Goetz A, Homeyer N, Izadi S, Janowski P, Kaus J, Kovalenko

- A, Lee T, LeGrand S, Li P, Lin C, Luchko T, Luo R, Madej B, Mermelstein D, Merz K, Monard G, Nguyen H, Nguyen H, Omelyan I, Onufriev A, Roe D, Roitberg A, Sagui C, Simmerling C, Swails J, Walker R, Wang J, Wolf R, Wu X, Xiao L, York D and Kollman P 2016 Amber 2016 university of California, San Francisco
- [54] Jakalian A, Jack D B and Bayly C I 2002 *Journal of Computational Chemistry* **23** 1623–1641 ISSN 1096-987X URL <http://dx.doi.org/10.1002/jcc.10128>
- [55] Tokui S, Oono K, Hido S and Clayton J 2015 Chainer: a next-generation open source framework for deep learning *NIPS* URL http://learningsys.org/papers/LearningSys_2015_paper_33.pdf
- [56] The HDF Group 1997-2017 Hierarchical Data Format, version 5 accessed: May 05, 2017 URL <http://www.hdfgroup.org/HDF5/>
- [57] Golkov V, Skwark M J, Mirchev A, Dikov G, Geanes A R, Mendenhall J, Meiler J and Cremers D 2017 *ArXiv e-prints* (*Preprint* 1704.04039)
- [58] He K, Zhang X, Ren S and Sun J 2015 *CoRR* **abs/1502.01852** URL <http://arxiv.org/abs/1502.01852>
- [59] Kingma D P and Ba J 2014 Adam: A method for stochastic optimization accessed: 2017-04-04 (*Preprint* 1412.6980) URL <http://arxiv.org/abs/1412.6980v9>
- [60] Tieleman T and Hinton G 2012 Coursera: Neural networks for machine learning, lecture 6.5 – rmsprop accessed: 2017-04-04 URL http://www.cs.toronto.edu/~tijmen/csc321/slides/lecture_slides_lec6.pdf
- [61] Funk S 2015 Smorms3 - blog entry: Rmsprop loses to smorms3 - beware the epsilon! accessed: 2017-04-04 URL <http://sifter.org/simon/journal/20150420.html>
- [62] Chen T and Guestrin C 2016 *CoRR* **abs/1603.02754** URL <http://arxiv.org/abs/1603.02754>
- [63] Sheridan R P, Wang W M, Liaw A, Ma J and Gifford E M 2016 *Journal of Chemical Information and Modeling* **56** 2353–2360 pMID: 27958738
- [64] Sosnin S 2017 Clever URL dx.doi.org/10.5281/zenodo.835526
- [65] Chemaxon 2016 Instant jchem 17.1.16.0 URL <http://www.chemaxon.com>

Supporting information for: Predicting bioaccumulation using molecular theory: A machine learning approach

Sergey Sosnin,[†] Maksim Misin,[‡] and Maxim V. Fedorov^{*,†}

[†]*Skolkovo Institute of Science and Technology, Skolkovo Innovation Center, Moscow
143026, Russia*

[‡]*Institute of Chemistry, University of Tartu, Ravila 14a, Tartu 50411, Estonia*

E-mail: m.fedorov@skoltech.ru

Conformer generation

We used two sets: C_{gen} and C_{keep} . C_{gen} was a set of the generated conformers and C_{keep} was a set with selected conformers. Initially, we calculated the energies of all conformers and select the lowest one C_{low} . Then we moved the C_{low} conformer from C_{gen} to C_{keep} . After that we estimated the $RMSD$ between each conformer in C_{gen} and each one in C_{keep} and moved from C_{gen} to C_{keep} only conformers with $RMSD$ more than predefined threshold (with threshold equal to 0.3 Å). Selected conformers have been saved as PDB files for future partial charges calculations and 3D RISM routines. Another selection approach, based on Taylor and Butina clustering algorithm,^{S1} resulted in significantly worse results. Our experiments revealed that the standardization of the orientation of the conformers is a crucial step for future modeling. For standardizations, all conformers of each molecule have been orientated such the principal axes of the molecule have been aligned with the x, y, z axes.

ActivNet4 architecture

Table S1: The architecture of *ActivNet4*. *convX* denotes a 3D convolution layer, *poolX* layer denotes a 3D max-pulling layer, and *fcX* denotes a fully-connected layer, where *X* is the sequential number of the layer.

Layer	Kernel or pool size	Activation
conv1	(3, 3, 3)	prelu
pool1	(2, 2, 2)	–
conv2	(3, 3, 3)	prelu
pool2	(2, 2, 2)	–
conv3	(3, 3, 3)	prelu
pool3	(2, 2, 2)	–
conv4	(3, 3, 3)	prelu
pool4	(2, 2, 2)	–
Dense layer	Neurons	Activation
fc1	1024	prelu
output	1	–

Parameters of optimizers

To train our networks we used the parameters listed below. For *Adam* optimizer $\alpha = 0.001$, $\beta_1 = 0.9$, $\beta_2 = 0.999$, $\epsilon = 1e - 08$ parameters have been set. For *RMSProp* we used *learning rate* = 0.01, $\alpha = 0.001$, $\epsilon = 1e - 08$ values. For Stochastic gradient descent we used *learning rate* = 0.01, *momentum* = 0.9. All other parameters were set to default.

Comparison of calculation time on CPU and GPU

We compared the code for the electric potential calculations written for execution on CPU and GPU. We have performed CPU test on Intel(R) Core(TM) i7-6700 CPU with frequency up to 3.40GHz. We implemented the code in *numpy* (CPU) and *cupy* (a part of *chainer* framework^{S2}) (GPU) versions. GPU tests have been performed on GeForce GTX 1080 card. We concluded that the GPU version is from 20 to 30 times faster than the CPU one, for the wide range of molecule sizes.

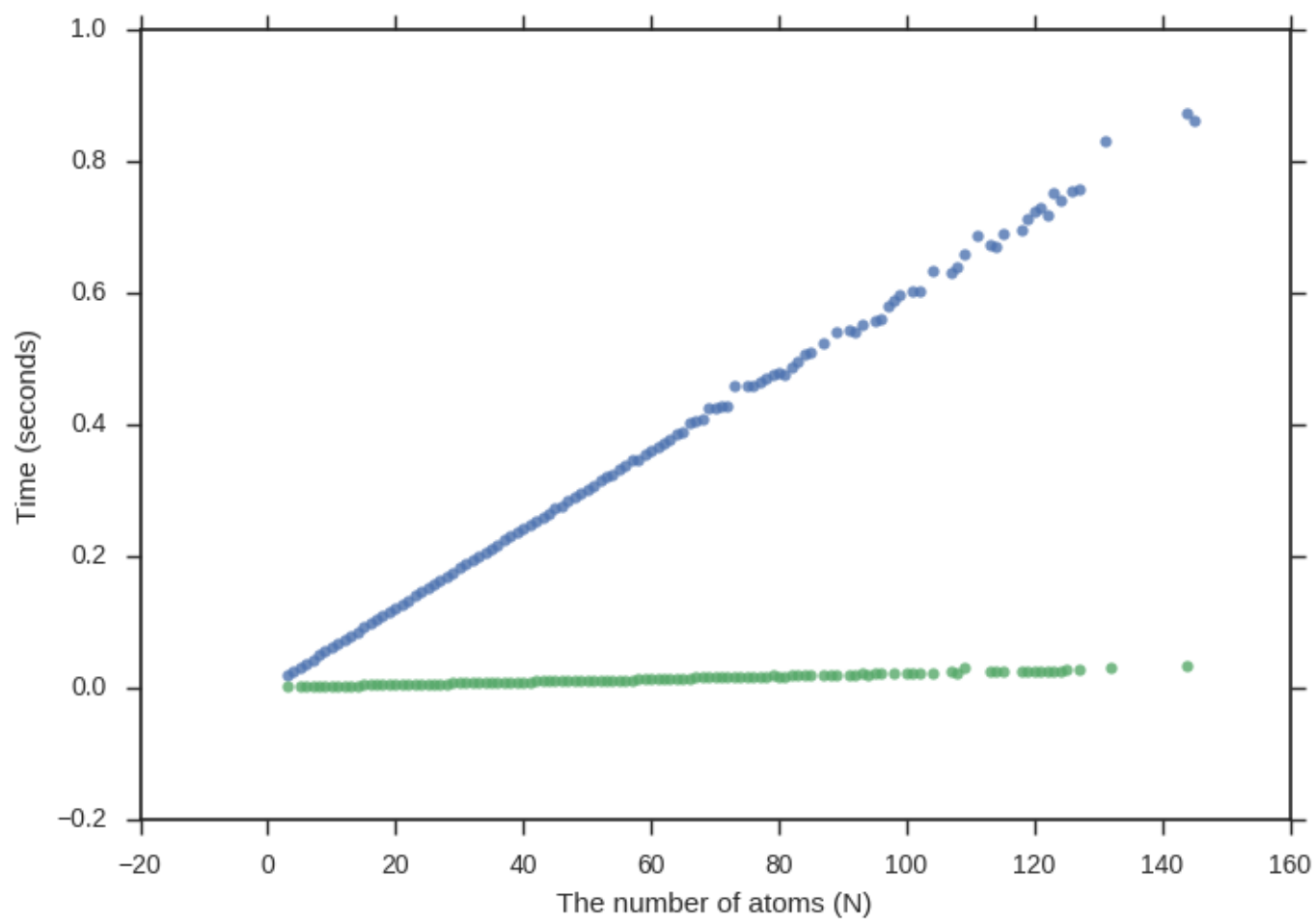


Figure S1: Comparison of calculation time on CPU (blue) and GPU (green) depending on the number of atoms in molecule (N).

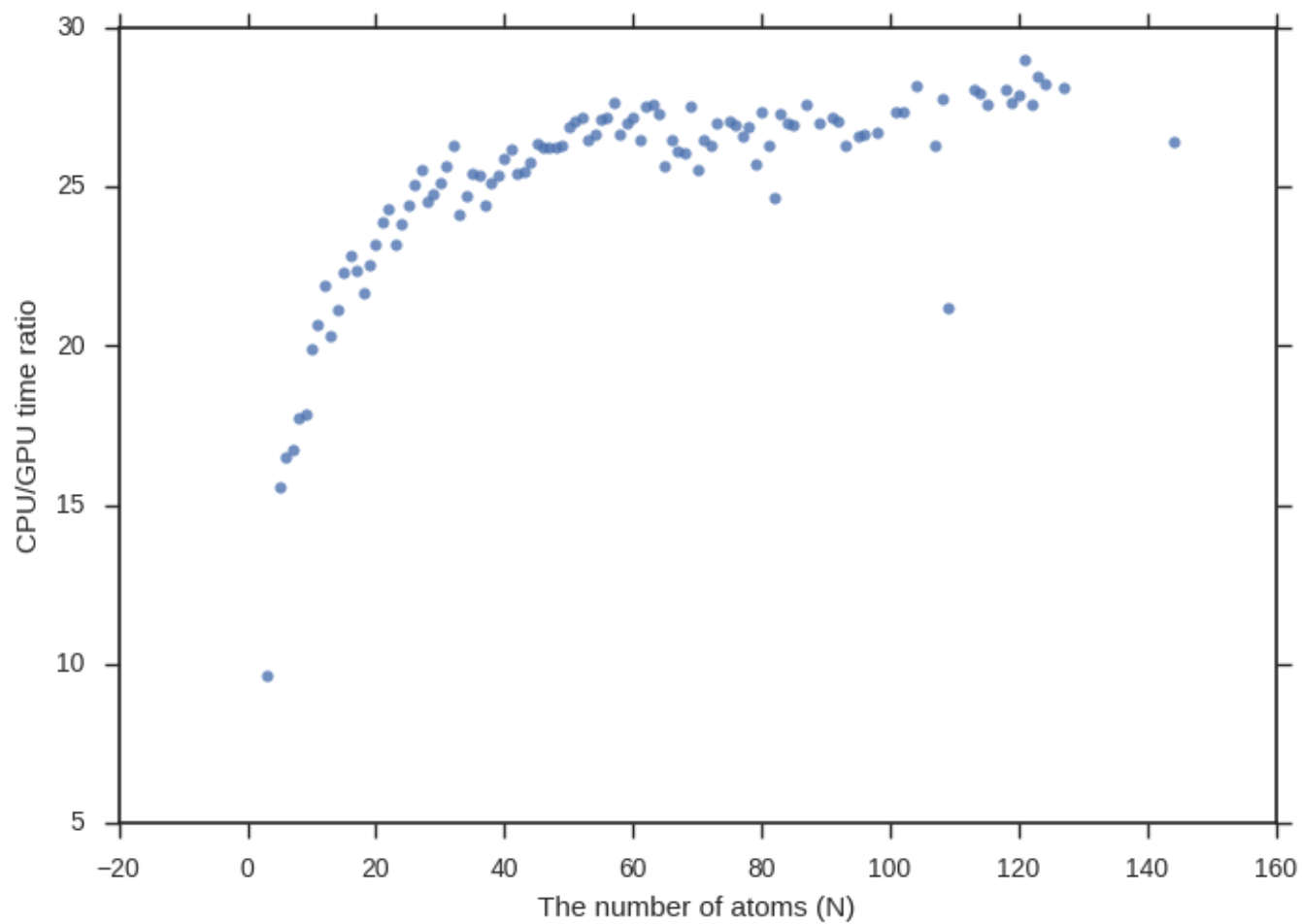


Figure S2: Ratio of calculation time on CPU to calculation time on GPU depending on the number of atoms in molecule (N).

References

- (S1) Butina, D. Unsupervised Data Base Clustering Based on Daylight’s Fingerprint and Tanimoto Similarity: A Fast and Automated Way To Cluster Small and Large Data Sets. *Journal of Chemical Information and Computer Sciences* **1999**, *39*, 747–750.
- (S2) Tokui, S.; Oono, K.; Hido, S.; Clayton, J. Chainer: a Next-Generation Open Source Framework for Deep Learning. NIPS. 2015.